

IOPS: An Unified SpMM Accelerator Based on Inner-Outer-Hybrid Product

Wenhao Sun , Wendi Sun , Song Chen, *Member, IEEE*, and Yi Kang

Abstract—Sparse matrix multiplication (SpMM) is widely applied to numerous domains, such as graph processing, machine learning, and data analytics. However, inner product based SpMM induces redundant zero-element computing for mismatched nonzero operands, while outer product based approach lacks input reuse across Process Elements (PEs) and poor output locality for accumulating partial sum (psum) matrices. Besides, current works only focus on sparse-sparse matrix multiplication (SSMM) or sparse-dense matrix multiplication (SDMM), rarely performing efficiently for both. To address these problems, this paper proposes an unified SpMM accelerator, called IOPS, hybridizing inner with outer products. It reuses the input matrix among PEs with inner product dataflow, and removes zero-element calculations with outer product approach in each PE, which can efficiently process SSMM and SDMM. Moreover, an address mapping method is designed to accumulate the irregular sparse psum matrices, reducing the latency and DRAM access of psum accumulating. Furthermore, an adaptive partition strategy is proposed to tile the input matrices based on their sparsity ratios, effectively utilizing the storage of architecture and reducing DRAM access. Compared with the SSMM accelerator, SpArch, we achieve $1.7\times\sim 6.3\times$ energy efficiency and $1.2\times\sim 4.4\times$ resource efficiency, with $1.4\times\sim 2.1\times$ DRAM access saving.

Index Terms—Sparse matrix multiplication, accelerator, Inner-Outer Product.

1 INTRODUCTION

SpMM is the key computing kernel for many applications, such as shortest-paths search [1], recommendation systems [2], molecular dynamics [3], and graph computing [4]. Since the density of sparse matrices is as low as $10^{-3}\sim 10^{-6}$ [5], removing zero-element calculations can greatly enhance system performance and energy efficiency.

Currently, SpMM is calculated based on inner or outer product approach. For inner product, its computation pattern is dot product between each row of matrix A and each column of matrix B to obtain an element of output matrix, which can fully reuse the output matrix. To increase the reuse of input matrices, inner product calculations are often mapped to systolic arrays, such as TPU [6], RASA [7]. However, the mismatched positions of nonzero elements in the input matrix introduce a large number of zero element calculations, causing degradation of performance and energy efficiency. Zhu et al [8] and RP-GCN [9] adopt an offline clustering approach to compress the sparse adjacency matrix into multiple dense matrices. However, this pre-processing step takes excessive time in the whole process, resulting in low performance of overall system. HyGCN [10]

proposes a static graph partition for data reuse and dynamic sparsity elimination to reduce redundant accesses. SPOTS [11] removes the all-zero rows or columns of input matrix through bitmap mask. But there still remain many zeros in the processed matrix, causing inefficient performance improvement.

For the outer product approach, the computation pattern is outer product between the columns of matrix A and the rows of matrix B to generate a psum matrix. This approach can overcome the irregular distribution of nonzero elements and theoretically skip all calculations of zero elements, thus significantly improving performance. However, the distribution of nonzero elements in each psum matrix is irregular, which involves enormous time and energy costs to accelerators, such as Dalton et al [12], Liu et al [13], Lee et al [14], MOSCON [15], and OuterSPACE [16]. To address the irregularity of psum matrix, SpArch [17] condenses the psum matrix with a Huffman Tree scheduler and accumulates them with a merge tree, accelerating the process of psum accumulation. AWB-GCN [18] and GCNAX [19] apply row remapping strategy to accumulate psum more regularly. MatRaptor [20] proposes a row-wise product approach, which computes the output matrix by row and achieves high resource efficiency. However, These works neglect data reuse among PEs, resulting in longer delay of data loading and lower overall performance.

The applications based on SpMM include not only SSMM, such as interior point methods [21], searching algorithms [22], and matching algorithms [23], but also SDMM, such as GCNs [4], GraphSage [24], GINConv [25], and GAT [26]. However, some work only accelerate the former, such as Zhu et al [8], AWB-GCN [18], and GCNAX [19], which can only exploit the sparsity of one matrix. Other works only focus on the acceleration of SSMM, such as OuterSPACE [16], SpArch [17], and MatRaptor [20], which aggravates

- This work was supported in part by the Strategic Priority Research Program of Chinese Academy of Sciences, Grant No. XDB44000000, in part by CAS Project for Young Scientists in Basic Research under grant No. YSBR-029k, and in part by the National Key R&D Program of China under grant No. 2019YFB2204800. The authors want to thank Information Science Laboratory Center of USTC for the hardware & software services.
- Wenhao Sun and Wendi Sun are affiliated with the School of Microelectronics, University of Science and Technology of China, Hefei, Anhui, 30332 China.
- Song Chen and Yi Kang are affiliated with the School of Microelectronics, University of Science and Technology of China, and also with the Institute of Artificial Intelligence, Hefei Comprehensive National Science Center, Hefei, Anhui, 30332 China.
(Corresponding author: Song chen, E-mail: songch@ustc.edu.cn)

the latency of input loading and psum accumulating due to data increment in SDMM. HyGCN [10] supports SSMM and dense-dense matrix multiplication (DDMM) by integrating two different computing engines, causing extra resource consumption for the interface and imbalanced workload in some cases between two engines.

To address these problems above, this paper proposed a unified SpMM accelerator based on inner-outer-hybrid product (IOHP), adaptive for various SpMM processing. Our main contributions are as follow:

1). To address the mismatched operands of inner product and lack of input reuse of outer product, we proposed an IOHP method for SpMM, which reuses the input matrix across PEs with inner product and removes zero-element calculations with outer product in each PE, and collaborated with an address mapping method to accumulate the irregular psum matrices, reducing the latency and DRAM access of psum accumulating.

2). To support both SSMM and SDMM computing, we designed an unified SpMM accelerator, called IOPS, whose procedure for SSMM consists of three pipeline stages: encoding input matrices with RP-CSC (Row Partition CSC) and CP-CSR (Column Partition CSR) format, calculating psum based on IOHP, accumulating psum through address mapping. For SDMM, we omit the last stage and reorganize the psum buffers to reduce DRAM access.

3). To optimize the DRAM access, we proposed an adaptive partition strategy to tile the input matrices based on their sparsity and size, effectively utilizing the storage of architecture and reducing DRAM access.

Compared with inner product based accelerator, SPOTS [11], we achieve $14.3\times\sim 43.7\times$ performance and $7.2\times\sim 21.9\times$ energy efficiency due to the IOHP approach. Compared with outer product based accelerator for SDMM, GCNAX [19], we achieve a similar performance in the SDMM benchmark and speed up by $9.8\times\sim 12.1\times$ in the SSMM benchmark because of the unified computing mode. For the outer product based accelerator for SSMM, SpArch [17], we achieve $1.3\times\sim 4.8\times$ performance and $1.7\times\sim 6.3\times$ energy efficiency for the efficient reuse of input matrices.

2 PRELIMERY

2.1 Compression Format of Sparse Matrix

Generally, the density of sparse matrix is quiet low. To reduce the storage cost, it is usually compressed with Compressed-Sparse-Column (CSC) format or Compressed-Sparse-Row (CSR) format, as shown in Fig.1.

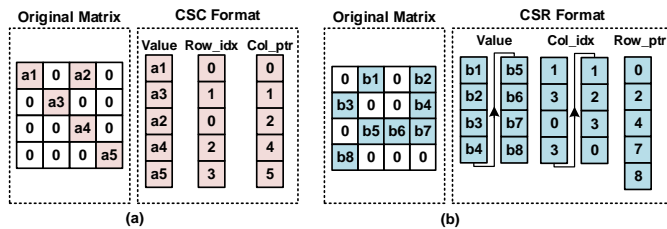


Fig. 1: Compression format of sparse matrix. (a)CSC format. (b)CSR format.

For the matrix of CSC format, it consists of *value*, *row_idx*, and *col_ptr*, where *row_idx* records the row index of element and *col_ptr* represents the start point of element in each column. For the matrix of CSR format, it consists of *value*, *col_idx*, and *row_ptr*, where *col_idx* records the column index of each element and *row_ptr* represents the start point of element in each row. Due to the lower storage cost, the matrices of CSC and CSR format are the appropriate input for SpMM.

2.2 Inner Product

Inner product is widely applied for regular matrix multiplication, which conducts a dot product between one row of matrix A and one column of matrix B, as shown in Fig.2(a). Assuming that the dimension of input matrix A, B, and output matrix C are $M \times K$, $K \times N$, $M \times N$, respectively, this approach can be mapped into a systolic array with high data reuse rate, where each row of matrix A, $A_row_i (i = 0, 1, \dots, M - 1)$, is shared by one row of PEs, and each column of matrix B, $B_col_j (j = 0, 1, \dots, N - 1)$, is shared by one column of PEs. For the PE of *i*-th row and *j*-th column, the operation can be expressed by Equ.1, obtaining one final result of matrix C.

Although the inner product can reuse the input matrices efficiently, the mismatched indexes of matrix A and B in the PE array will induce a large amount of zero-element computing for SpMM, degrading the performance dramatically. Thus, how to accelerate the inner product approach is worth exploring.

$$C[i, j] = \sum_{x=1}^{K-1} A[i, x] * B[x, j] \quad (1)$$

2.3 Outer Product

Outer product can naturally avoid the mismatched indexes, where an outer product is performed between one column of matrix A and one row of matrix B, as shown in Fig.2(b). In this approach, the *i*-th ($i = 0, 1, \dots, K - 1$) PE receives the *i*-th column of matrix A, A_col_i , and *i*-th row of matrix B, B_row_i , to obtain one psum matrix, as expressed by Equ.2. For each PE, it only needs to compute the non-zero elements, which achieves higher performance compared with inner product.

Although outer product can accelerate SpMM efficiently, there is no input matrix reusing among PEs, which requires $N \times$ bandwidth of loading input compared with inner product for an $N \times N$ PE array. Once the data loading speed is slower than the PE computation, the overall performance will also be degraded. Thus, how to enhance the input reusing of outer product is also a key challenge.

$$psum[a, b] = A[a, i] * B[i, b] \quad (a \in [0, M), b \in [0, N)) \quad (2)$$

3 INNER-OUTER-HYBRID PRODUCT

3.1 Computing flow for SSMM

To solve the problem of inner and outer product, we proposed an IOHP approach for SpMM acceleration, as shown in Fig.2(c). Firstly, the matrices A and B are respectively divided to G_{NA} groups in the row dimension and G_{NB} groups in the column dimension, and the specific

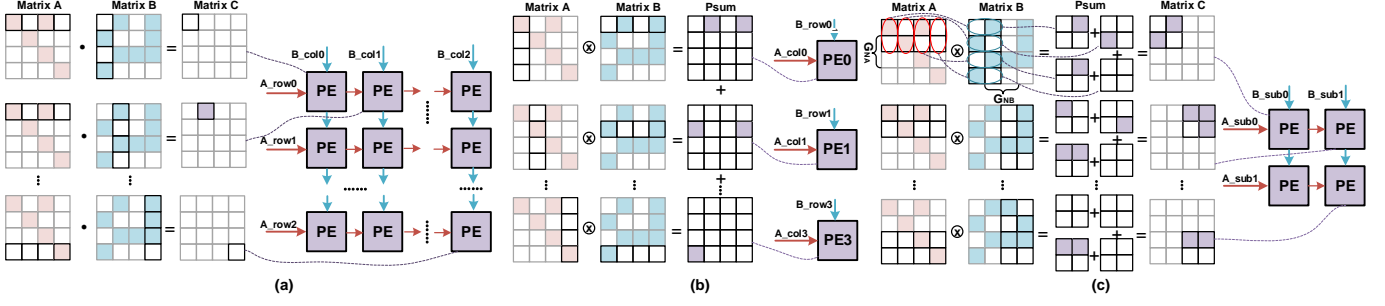


Fig. 2: Computing approach of SpMM. (a)Inner product. (b)Outer product. (c)IOHP.

partition method is explained in Section.5. Assuming that the size of tiled matrix A_{sub_i} ($i = 0, 1, \dots, G_{NA} - 1$) and B_{sub_j} ($j = 0, 1, \dots, G_{NB} - 1$) is $M_t \times K$ and $K \times N_t$ respectively, each A_{sub_i} and B_{sub_j} can be shared by the PEs in the same row and column respectively as the inner product approach. Then, the PE in i -th row and j -th column performs an outer product between a A_{sub_i} and B_{sub_j} , which is expressed in Eq.3 and can skip most zero-element calculations as outer product approach. Finally, we can both reuse the input matrix and improve the performance efficiently based on IOHP.

$$C[a, b] = \sum_{x=1}^{K-1} A[a, x] * B[x, b] \quad (3)$$

$$(a \in [i * M_t, (i + 1) * M_t], b \in [j * N_t, (j + 1) * N_t])$$

An example of IOHP computing is shown in Fig.3. First, the 4×4 input matrix A and B are divided into two 2×4 and 4×2 submatrices. Then, we extract the non-zero elements and their corresponding location from these submatrices. Finally, we load these input elements to perform outer product in each PE and obtain all psum elements. Compared with inner product, we achieve $1.8 \times$ speedup. Compared with outer product, we save $2 \times$ bandwidth of loading input matrix.

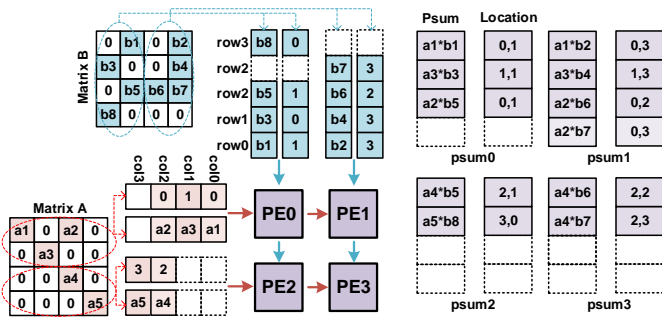


Fig. 3: An example of SSMM based on IOHP.

3.1.1 Encoding Format

To fit with the computing flow of IOHP, we need to transfer the original input matrices of CSC and CSR format to RP-CSC and CP-CSR respectively, as shown in Fig.4. For matrix A, apart from the value and row index, we need to record the length of non-zero elements in each column. Besides, after row partition, not every group of submatrix A contains non-zero elements in each column. Thus, we apply a group bitmap to record the empty/non-empty state of

each group in the current column. Finally, submatrix A of RP-CSC format consists of *value*, *row_idx*, *col_len*, *col_idx*, and *group_bitmap*, where the former three are stored in each group and the latter two are stored once for all groups. Similarly, submatrix B of CP-CSR format consists of *value*, *col_idx*, *row_len*, *row_idx*, and *group_bitmap*.

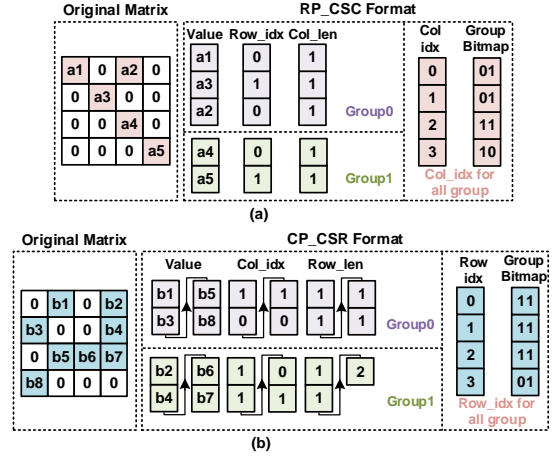


Fig. 4: Encoding format of matrix A and B. (a)RP-CSC format of matrix A. (b)CP-CSR format of matrix B.

The specific flow of encoding is shown in Tab.1. Since the sizes of input matrices in the real world are unpredictable, we need to tile them further in the row and column dimension. The detail is discussed in Section.5. After partition, we obtain $T_M \times T_K$ blocks of G_{NA} groups of $M_t \times K_t$ submatrix A, and $T_K \times N_K$ blocks of G_{NB} groups of $K_t \times N_t$ submatrix B in the 1~3-th line. For G_{NA} groups of $M_t \times K_t$ submatrix A, we encode them column-wise in the 5-th line. First, we locate the first element with *col_ptr_A* in the 7-th line. If the *row_idx_A* is in the range of row index of the current block, we figure out which group it belongs to in the 8-th line. Then, we copy the *value* and *row_idx* to the corresponding group in the 9-th line. The *col_len_sA* self-increases one and the *group_bitmap_sA* is set to 1'b1 in the 10~11-th line. When the *row_idx_A* is out of range, we update the original *col_ptr_A* with the current location and record the *col_idx_sA* in the 12~13-th line. After that, we repeat the above operations until all columns are traversed. Finally, we record the length of non-empty columns for all groups, *col_all_len_sA* in the 16-th line. For G_{NB} groups of $K_t \times N_t$ sub-matrix B, we encode them row-wise with similar operations in the 17~27-th line.

TABLE 1: Encoding flow of matrix A and B

Input: Matrix A of CSC: $value_A, row_idx_A, col_ptr_A$;
Matrix B of CSR: $value_B, col_idx_B, row_ptr_B$;
of tiling matrix A/B: T_M, T_K, T_N ;
of group submatrix A/B: G_{NA}, G_{NB} ;
Size of submatrix A/B: $M_t \times K_t, K_t \times N_t$.
Output: submatrix A of RP_CSC: $value_sA,$
 $row_idx_sA, col_len_sA, col_idx_sA, group_bitmap_sA$;
submatrix B of CP_CSR: $value_sB, col_idx_sB,$
 $row_len_sB, row_idx_sB, group_bitmap_sB$.

```

1  for(a = 0; a < T_M; a = a + 1)
2    for(b = 0; b < T_M; b = b + 1)
3      for(c = 0; c < T_K; c = c + 1)
4        Reset all variable
5        for(d = 0; d < K_t; d = d + 1)
6          ///// RP - CSC Encoding of matrix A /////
7            while(row_idx_A in a - th row - block)
8              group_id = row_idx_A / M_t
9              value_sA[group_id] = value_A
10             row_idx_sA[group_id] = row_idx_A
11             col_len_sA[group_id] ++
12             group_bitmap_sA[group_id] = 1'b1
13             e ++
14             col_all_id ++
15             col_ptr_A += e, col_idx_sA = d
16             col_all_len_sA = col_all_id
17             ///// CP - CSR Encoding of matrix B /////
18             f = 0
19             while(col_idx_B in b - th column - block)
20               group_id = col_idx_B / N_t
21               value_sB[group_id] = value_B
22               col_idx_sB[group_id] = col_idx_B
23               row_len_sB[group_id] ++
24               group_bitmap_sB[group_id] = 1'b1
25               f ++
26               row_all_id ++
27               row_ptr_B += f, row_idx_sB = d
28               row_all_len_B = row_all_id

```

3.1.2 Psum Calculation

After Encoding, we need to apply the encoded matrices to calculate psum, as shown in Tab.2. First, we read the column index of matrix A and row index of matrix B. If $col_idx_sA < row_idx_sB$, we move the col_idx_sA to next column in the 2~3-th line. If $col_idx_sA < row_idx_sB$, we move the row_idx_sB to next row in the 4~5-th line. If $col_idx_sA = row_idx_sB$, we can calculate the psum. First, for those groups with $group_bitmap = 1$, we fetch the elements of $value_sA$, $value_sB$, and col_idx_sB to calculate the psum value, $value_psum$, and column index, col_idx_psum , in the 13~14-th line. Besides, we store the memory address of $value_psum$ and col_idx_psum , id_psum , to the row_idx_sA segment of vc_addr_psum in the 15-th line. Additionally, we record the length of psum, row_len_psum , in the row_idx_sA row in the 16-th line so that we can access the psum row-wise regularly. When all elements in current col_idx_sA and row_idx_sB are finished, we traverse the remainings and repeat the above operations.

An example of psum calculation based on IOHP is shown in Fig.5, where the input matrix comes from Fig.3. At T_1 , due to $col_idx_sA = row_idx_sB = 0$, we read the $group_bitmap_sA$ and $group_bitmap_sB$, indicating that $group0$ of submatrix A, $group0$ and $group1$ of submatrix B are non-empty. Since the col_len_sA and row_len_sB are both 1, we fetch the $\langle value_sA, row_idx_sA \rangle = \langle$

$a1,0 \rangle, \langle value_sB, col_idx_sB \rangle = \langle b1,1 \rangle$, and $\langle value_sB, col_idx_sB \rangle = \langle b2,1 \rangle$ to calculate psum. Then, we move to the next column, $col_idx_sA = 1$ (also next row, $row_idx_sB = 1$) to execute similar operations at T_2 . The whole process takes 5 cycles. The bottom right corner shows the process of psum calculation from submatrix A of $group0$ and submatrix B of $group1$. The $value_psum$ and col_idx_psum are stored in the order of $T_1 \sim T_4$. Assuming the maximum length of non-zero psum is 4, the memory addresses of $value_psum$ and col_idx_psum in $row0$ are stored in $address0 - 3$ of vc_addr_psum and $row1$ in $address4 - 7$. Besides, the row_len_psum are stored in the order of row index. Based on the vc_addr_psum and row_len_psum , we can access the psum of each row regularly.

TABLE 2: Computing Flow of Psum

Input: submatrix A of RP_CSC: $value_sA, row_idx_sA,$
 $col_len_sA, col_idx_sA, group_bitmap_sA$;
submatrix B of CP_CSR: $value_sB, col_idx_sB,$
 $row_len_sB, row_idx_sB, group_bitmap_sB$.
Output: psum: $value_psum, col_idx_psum,$
 $row_len_psum, addr_col_psum$.

```

1  while(col_id < col_all_len_sA &
2    row_id < row_all_len_sB)
3    if(col_idx_sA < row_idx_sB)
4      ena_gb = 1, enb_gb = 0
5    elseif(col_idx_sA[col_id] < row_idx_sB[row_id])
6      ena_gb = 0, enb_gb = 1
7    else
8      ena_gb = 1, enb_gb = 1
9    for(g = 0; g < G_NA; g = g + 1)
10     for(h = 0; h < G_NB; h = h + 1)
11       if(ena_gb == 1 & group_bitmap_sA[g] == 1
12         & enb_gb == 1 and group_bitmap_sB[h] == 1)
13         for(i = 0; i < col_len_sA[g]; i = i + 1)
14           for(j = 0; j < row_len_sB[h]; j = j + 1)
15             value_psum[g][h] = value_sA[g]*
16               value_sB[h]
17             col_idx_psum[g][h] = col_idx_sB[h]
18             vc_addr_psum[g][h][row_idx_sA[g]] =
19               id_psum[g][h]
20             row_len_psum[g][h][row_idx_sA[g]] ++
21             id_psum[g][h] ++
22             col_id += ena_gb, row_id += enb_gb

```

3.1.3 Address Mapping

After calculating all Psums, we need to sort and accumulate the irregular psums to obtain the output matrix C as shown in Tab.3. For the $M_t \times N_t$ psum matrices, we traverse them row-wise in the 3-th line. First, we read the row_len_psum in the 4-th line. If $row_len_psum > 0$, we fetch the memory address of $col_idx_psum, vc_addr_psum$, in the 5~6-th line. Then, we read the col_idx_psum based on vc_addr_psum and sort them in the current row in the 7~8-th line. Based on the sorted memory address, $sorted_vc_addr_psum$, we read the $value_psum$ and accumulate the adjacent psum with the same col_idx_psum in the 9-th line. After that, we obtain the final result of matrix C, $\langle value_C, row_idx_C, col_idx_C \rangle$ in the 10-th line. When all psum are traversed, we can encode them with the standard CSC or CSR format in the 11-th line.

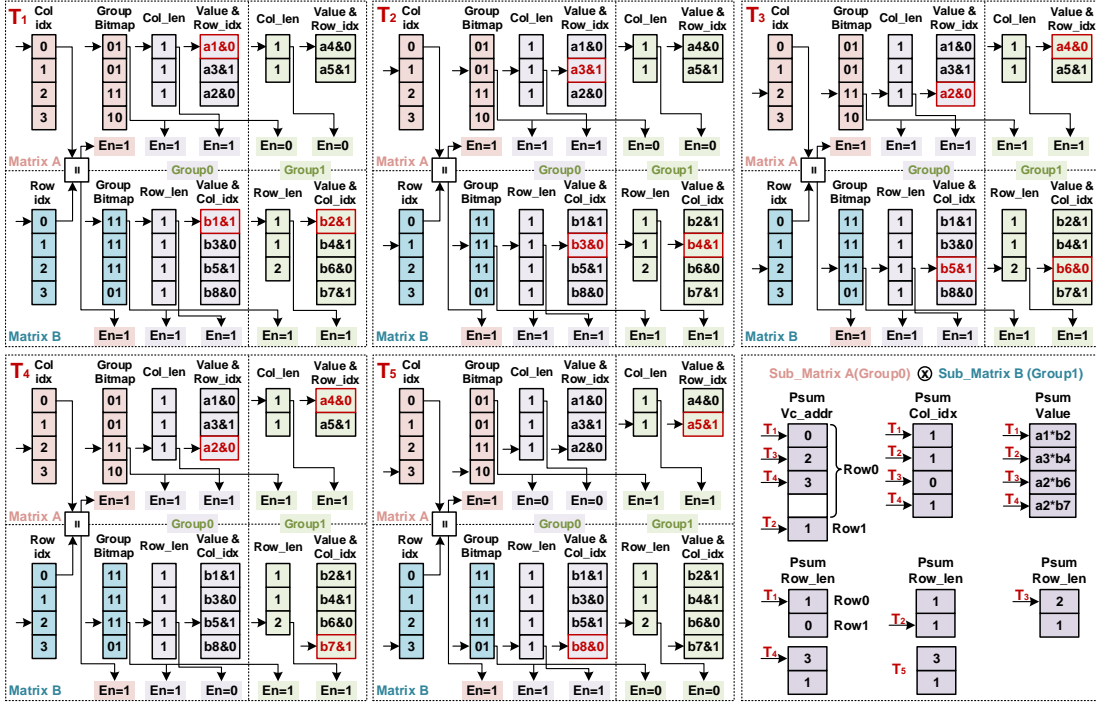


Fig. 5: An example of psum calculation.

TABLE 3: Computing Flow of Address Mapping

Input: psum: $value_psum, col_idx_psum, row_len_psum, vc_addr_psum$.	
Output: Matrix C of CSC (or CSC) format.	
1	$for(g = 0; g < G_{NA}; g = g + 1)$
2	$for(h = 0; h < G_{NB}; h = h + 1)$
3	$for(i = 0; i < M_i; i = i + 1)$
4	$if(row_len_tmp[g][h] > 0)$
5	$vc_addr_tmp = vc_addr_psum[g][h]$
6	$col_idx_tmp = col_idx_psum[g][h]$
7	$(sorted_vc_addr_tmp, sorted_col_idx_tmp)$
	$= sort(vc_addr_tmp, col_idx_tmp)$
8	$value_C_tmp = value_psum[g][h]$
9	$accum(value_C_tmp, sorted_col_idx_tmp)$
10	$(value_C, row_idx_C, col_idx_C)$
	$= (value_C_tmp, i, sorted_col_idx_tmp)$
11	$Encode_CSC(value_C, row_idx_C, col_idx_C)$

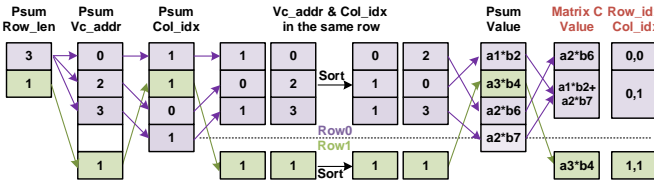


Fig. 6: An example of address mapping.

An example of address mapping is shown in Fig.6. The row_len_psum of row0 and row1 are 3 and 1 respectively. For row0, we fetch the $col_idx_psum = \langle 1, 0, 1 \rangle$ based on the $vc_addr_psum = \langle 0, 2, 3 \rangle$. Then, we sort the col_idx_psum with corresponding vc_addr_psum . After that, we fetch the $value_psum = \langle a1 * b2, a3 * b4, a2 * b6 \rangle$ based on the sorted $vc_addr_psum = \langle 2, 0, 3 \rangle$. The $value_psum = a1 * b2$ and $a2 * b6$ are accumulated due to the same col_idx_psum . Finally, we obtain the value and loca-

tion of matrix C, $\langle value_C, row_idx_C, col_idx_C \rangle = \langle (a2 * b6, 0, 0), (a1 * b2 + a2 * b7, 0, 1), (a2 * b6, 1, 1) \rangle$. For row1, we execute the similar operations, the $\langle value_C, row_idx_C, col_idx_C \rangle = \langle (a3 * b4, 1, 1) \rangle$.

3.2 Computing flow for SDMM

For SDMM, we can simplify the flow of IOHP, as shown in Tab.4. First, we only need to encode matrix A with RP-CSC format. Then, we fetch the value of matrix B, $value_B$, according to the column index of matrix A, col_idx_sA , in the 2-th line. Thus, we calculate column-wise. Since the psum matrix is dense, the location of each element is also regular. For those groups with $group_bitmap = 1$, we calculate the $value_psum$ and accumulate with the old psum in the 9-th line. When all elements are finished, we obtain a dense matrix C.

TABLE 4: Computing flow of SDMM based on IOHP

Input: Matrix A of CSC format: $value_A, row_idx_A, col_ptr_A$; Matrix B.	
Output: Matrix C.	
1	$Encode_RP_CSC(value_A, row_idx_A, col_ptr_A)$
2	$value_sB = value_B[col_idx_sA]$
3	$while(col_id < col_all_len_sA)$
4	$for(g = 0; g < G_{NA}; g = g + 1)$
5	$for(h = 0; h < G_{NB}; h = h + 1)$
6	$if(group_bitmap_sA[g] == 1)$
7	$for(i = 0; i < col_len_sA[g]; i = i + 1)$
8	$for(j = 0; j < N_i; j = j + 1)$
9	$value_psum[g][h] +=$
	$value_sA[g] * value_sB[h]$
10	$col_id ++$

Fig.7 shows an example of SDMM based on IOPS. First, the matrix A is encoded with RP-CSC format. Then,

we fetch the row_0, row_1, row_3 of matrix B based on the $col_idx_sA = \langle 0, 1, 3 \rangle$. After that, we calculate the psum to obtain matrix C. At T_1 , we calculate the $value_psum = a_1 * b_1$ and store it to $address = 0$. At T_5 , we get $value_psum = a_2 * b_7$ and accumulate with $value_psum = a_1 * b_1$ of $address = 0$. The whole process take 6 cycles and obtain a 2×2 dense matrix C.

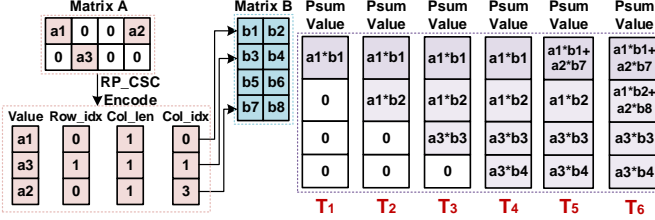


Fig. 7: An example of SDMM based on IOHP.

4 ARCHITECTURE

4.1 Top-level Architecture

To implement the IOHP approach, we design a hardware architecture, IOPS, as shown in Fig.8. It mainly consists of RP-CSC encoder, CP-CSR encoder, input buffers for matrices A and B (Buffer A, B), a PE array, address mapping modules (Addr Map), a top controller and a direct memory access (DMA) module. Initially, we load the original input matrices from DRAM to the encoders through DMA. Then, we encode the input matrices with RP-CSC and CP-CSR format and transfer the encoded matrices to buffer A and B. After that, the encoded matrices are fetched to PE array to calculate psum based on IOHP. Finally, the psum are sorted and accumulated regularly to obtain the output matrix C in the address mapping module, which also can be encoded with CSC or CSR format. To improve performance, we organize three major stages, encoding input matrices with RP-CSC and CP-CSR format, calculating psum based on IOHP, and accumulating psum through address mapping, as a pipeline structure. Besides, we can switch the computing mode between SSMM and SDMM to adapt different applications.

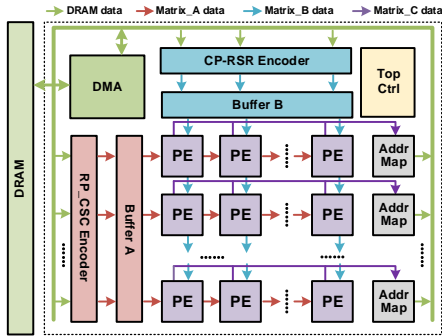


Fig. 8: Top-level architecture of IOPS.

4.2 PE array and Address Mapping Module

The PE array, the core of IOPS, is in charge of SpMM, which consists of $G_{NA} \times G_{NB}$ PE units. Each PE consists of a float-point multiplier and adder (FP-mult and FP-Add),

two sets of row_len buffers, value buffers, vc_addr buffers, and col_idx buffers. One set of buffers are applied to store the data during calculating psum as shown in Fig.9(a). The other set of buffers are used for fetching psum to obtain the output matrix collaborating with address mapping module as shown in Fig.9(b) and Fig.9(c).

To sort the location of psum, we equip two sequences of shift registers (idx/addr reg), comparators ($>?$), and multiplexer logic as shown in Fig.9(b). First, we fetch a col_idx_psum and a vc_addr_psum from buffers and compare the col_idx_psum with all registers. If the col_idx_psum is larger than the current register, we keep the original value. If the col_idx_psum is smaller than the current register while larger than the former one, the col_idx_psum and vc_addr_psum are inserted to the location of current register and the remaining registers shift right. After sorting, we read the $value_psum$ one by one from value buffer based on the sorted vc_addr_psum (sorted addr reg) as shown in Fig.9(c). Meanwhile, the sorted col_idx_psum (sorted idx reg) are fetched serially to detect the equality of the current and the former data. If equal, the $value_psum$ is accumulated with the former one. Otherwise, the former $value_psum$ is output as a final result of matrix C.

For the computing mode of SDMM, since the buffers corresponding to address mapping operation are idle, they can be merged with value buffers for a larger storage as shown in Fig.9(d). With more on-chip buffers, the size of submatrix becomes larger, obviously reducing the tiling blocks and lowering DRAM access further. Finally, we apply two value buffers to accumulate psum with a ping-pong buffer structure.

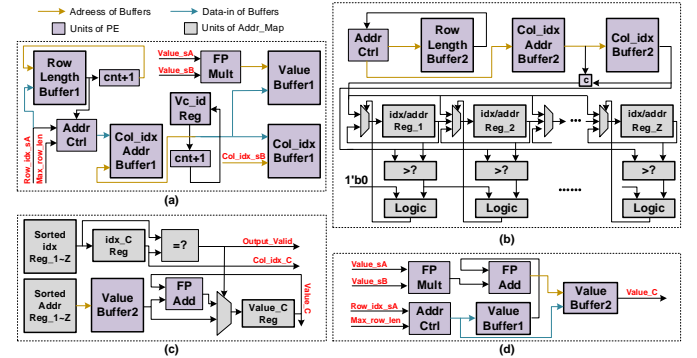


Fig. 9: PE and address mapping unit. (a) Calculating psum. (b) Sorting the location of psum. (c) Accumulating psum. (d) Computing mode of SDMM.

5 ADAPTIVE PARTITION STRATEGY

To reduce the DRAM access of overall architecture, we propose an adaptive partition strategy. Based on IOHP, we partition the matrix A and matrix B as shown in Fig.10. The specific partitioning parameters are shown in Tab.5. Matrix A and B are partitioned into $T_M \times T_K$ blocks of A_1 and $T_K \times T_N$ blocks of B_1 , respectively. Each A_1 contains G_{NA} groups of A_2 and each B_1 contains G_{NB} groups of B_2 , where each A_2 and B_2 are shared by the PEs in the same row and column, respectively. Each PE performs an outer

product between A_2 and B_2 , obtaining an output submatrix C_2 with the size of $M_t \times N_t$.

TABLE 5: Parameters of Data Partition

Parameter	Explanation
C_{psum}	capacity of psum buffer
C_A/C_B	capacity of input buffer A/B
M_A/M_B	storage size of matrix A/B
$M \times K$	size of matrix A
$K \times N$	size of matrix B
D_A/D_B	density of matrix A/B
G_{NA}/G_{NB}	group # of matrix A2/B2
R_x	reserved storage ratio of buffer
T_M	tiling # of matrix A row
T_K	tiling # of matrix A column (matrix B row)
T_N	tiling # of matrix B column
$M_t \times K_t$	size of submatrix A2
$K_t \times N_t$	size of submatrix B2

According to the partition method in Fig.10 and Tab.5, we need to solve a set of tiling parameters to minimize the DRAM access with limited buffer capacity. The specific algorithm is shown in Tab.6. Assuming an uniform distribution of sparsity in the input matrix, the M_t , K_t and N_t should satisfy constraints (1) – (3), which are the capacity limitations of buffer A, B, and psum, respectively. Generally, we reserve R_x free storage space due to the deviation between theory and reality. If it still exceeds the capacity of on-chip buffers, we will stop computing and load the psum of overflowed buffer into DRAM or read the rest input matrices from DRAM, which rarely happens. If the input buffer is capacious enough to store the submatrix A of $M_t \times K$ or B of $K \times N_t$, we can reuse matrix A first (RAF) or B first (RBF) to avoid repeat access, as shown in DrA_0 and DrA_1 . Otherwise, we reuse matrix A and B equally (RABE) and the DRAM access is calculated as DrA_2 . Finally, since the solution space of tiling parameter is limited, we apply the exhaustion method to solve it for minimizing DRAM access.

TABLE 6: Strategy of Data Partition

Input	$C_{psum}, C_A, C_B, M_A, M_B, R_x$ $M, K, N, D_A, D_B, G_{NA}, G_{NB}$
Output	$T_M, T_K, T_N, M_t, K_t, N_t$
Constraint	(1) $M_t \times K_t \times D_A < C_A \times R_x$ (2) $K_t \times N_t \times D_B < C_B \times R_x$ (3) $M_t \times D_A \times N_t \times D_B \times K_t < C_{psum} \times R_x$
Extra Condition	(a) $M_t \times K \times D_A < C_A \times R_x$ (b) $N_t \times K \times D_B < C_B \times R_x$
Target	$Min(DrA_0, DrA_1, DrA_2)$, where RAF : $DrA_0 = M_B \times T_M + M_A$, if (a) RBF : $DrA_1 = M_A \times T_N + M_B$, if (b) RABE : $DrA_2 = M_A \times T_N + M_B \times T_M$
Algorithm	exhaustion method

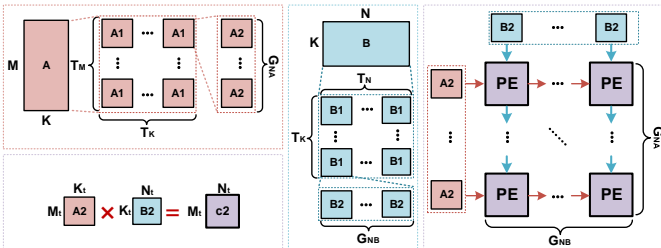


Fig. 10: Adaptive partition strategy.

6 EXPERIMENT

6.1 Implementation

IOPS implementation: To measure the area, power, and performance of hardware, we implemented IOPS in Verilog and conducted a functional simulation on Cadence Xcelium 2019.2. Then, the Verilog code was synthesized with Synopsys Design Compiler under the 65-nm technology. The on-chip SRAM buffers are generated by Memory Compiler and the power is calculated by Synopsys Prime Suite 2020.09.

The PE array is 8×8 , achieving a peak throughput of $64 \times 0.8GHz = 51.2GOP/s$. For original input matrix, the value, location, and data length are encoded in 64-bit (double float), 32-bit, and 16-bit, where these data of RP-CSC and CP-CSR format are encoded in 64-bit, 16-bit, and 8-bit, respectively. To balance performance and hardware overhead, the sizes of each data buffer are set as shown in Tab.7, where all of them are doubled as a ping-pong buffer structure. In SDMM mode, the buffer of `col_idx`, `row_len`, and `vr_addr` can be merged to an additional $256 \times 64b$ value buffer, which expands the on-chip storage and reduces the DRAM access. For the area and power breakdown of each module, PE array consumes 58.3% area and 65.4% power for calculating SpMM and storing psum data. Input buffers mainly store input matrices of RP-CSC and CP-CSR format, accounting for 32.2% area and 22.8% power. The Encoders provide a buffer for the original input matrices to encode them, with 7.2% area and 7.2% power consumption. Other parts such as controller and address mapping module are in charge of dataflow control and psum regularization, occupying only 2.4% area and 4.6% power.

TABLE 7: Area and Power of Each Module

Module	Area(mm2)	Power(W)	Buffer Size
PE Array	9.8 (58.2%)	2.09 (65.4%)	value: 256x64b, col_idx: 256x16b, row_len: 2x256x8b, vr_addr: 4x256x8b
Buffer A	2.7 (16.1%)	0.36 (11.4%)	value: 2Kx64b, row_idx: 2Kx16b, col_len: 2Kx8b, col_idx: 8Kx32b, bitmap: 8Kx16b
Buffer B	2.7 (16.1%)	0.36 (11.4%)	value: 2Kx64b, col_idx: 2Kx16b, row_len: 2Kx8b, row_idx: 8Kx32b, bitmap: 8Kx16b
Encoder A	0.6 (3.6%)	0.12 (3.6%)	value: 256x64b, row_idx: 256x32b, col_ptr: 256x16b
Encoder B	0.6 (3.6%)	0.12 (3.6%)	value: 256x64b, col_idx: 256x32b, row_ptr: 256x16b
Others	0.4 (2.4%)	0.15 (4.6%)	-
Total	16.8 (100%)	3.2 (100%)	-

To validate the superiority of this work, we set some baseline accelerators as shown in Tab.8, including inner and outer product based architectures, as well as SSMM and SDMM accelerators. The benchmark is shown in Tab.9. For SSMM, we testified with some real world sparse matrices in SNAP datasets [5], where the SSMM is calculated by the adjacent matrix (A) and feature matrix (X). For SDMM, we

TABLE 8: Overall Comparison of Each Accelerator

Accelerators	Technology (nm)	Technology Scalar (Area/Power)	PE Array Size	Area (mm ²)	Frequency (MHz)	Power (W)	Computing Approach	Expertise Domains
SPOTS [11]	45	2x/1.6x	4x128	8.6	500	1.1	Inner Product	DDMM
HyGCN [10]	12	29.3/23.4	8x4x128 32x16	7.8	1000	6.7	Inner Product	DDMM SSMM
GCNAX [19]	40	2.6x/2.1x	1x16	6.5	1000	0.37	Outer Product	SDMM
OuterSPACE [16]	32	4.1x/3.3x	16x16	87	1000	12.39	Outer Product	SSMM
SpArch [17]	40	2.6x/2.1x	16x16	28.49	1000	9.26	Outer Product	SSMM
IOPS	65	1x/1x	8x8	16.8	800	3.2	Inner-Outer Product	SSMM SDMM

testified with a 2-layer GCN model [4] on the Cora [27], Citeseer [28], Pubmed [29], Nell [30], and Reddit [31] datasets, where the SDMM is conducted by $A((A(XW_1))W_2)$ and the weight matrices, W_1, W_2 , are dense.

TABLE 9: Matrix Density and Demension of Each Dataset

Dataset	Vertex (A), Feature (X)	Density of A, X	Weight matrix W1,W2
cora	2708, 1433	0.14%, 1.27%	[1433,16], [16,7]
citeseer	3327, 3703	0.083%, 0.85%	[3703,16], [16,6]
pubmed	19717, 500	0.023%, 10%	[500,16], [16,3]
nell	169343, 61278	0.0041%, 0.011%	[61278,64], [64,186]
Reddit	232965, 602	0.021%, 51.6%	[602,64], [64,41]
Facebook	22470, 4714	0.034%, 0.3%	-
Deezer	28281, 30978	0.011%, 0.11%	-
Twitch	9498, 2514	0.17%, 0.81%	-
Wiki	11631, 13183	0.25%, 0.84%	-
Github	37700, 4005	0.04%, 0.46%	-

6.2 Performance

To demonstrate the superiority of IOPS, we compared the performance with the SPOTS [11], HyGCN [10], GCNAX [19], OuterSPACE [16], and SpArch [17], achieving $14.3\times\sim 43.7\times$, $3.2\times\sim 19.8\times$, $0.72\times\sim 12.1\times$, $2.9\times\sim 6.4\times$, and $1.3\times\sim 4.8\times$, respectively, as shown in Fig.11. To eliminate the influence of hardware scale and technology node, the normalized performance, P_N , is calculated as R_{Pr}/R_{Pt} , where R_{Pr} and R_{Pt} are the ratios of real performance and top performance of IOPS to other accelerators, respectively.

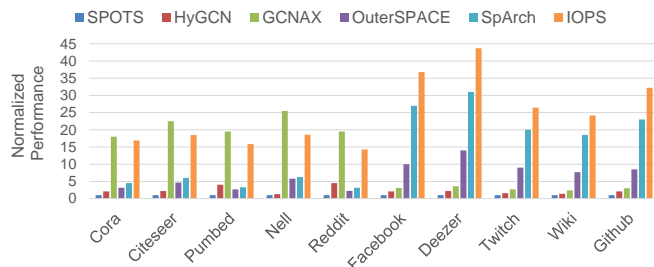


Fig. 11: Performance comparison with SPOTS, HyGCN, GCNAX, OuterSPACE, and SpArch.

For SPOTS, it reuses the input matrices across PEs array based on inner product and improves the performance by removing the rows and columns with all zeros. However, this approach can only skip minority zero computing due to the mismatched index between input matrix A and B. Compared with SPOTS, we conduct the outer product in each PE to avoid the problem. Thus, our performance is $14.3\times\sim 43.7\times$ higher than SPOTS.

For HyGCN, it integrates the SIMD cores for SSMM and systolic arrays for DDMM. The window shrinking method of HyGCN dynamically eliminates the sparsity of the inner-product based computing kernel. For SSMM benchmark, the DDMM computing engine works like SPOTS in the best case. For SDMM benchmark, the execution order of $(A \times X) \times W$ causes increment of operation compared with $A \times (X \times W)$. Besides, the workloads between two computing engines can be imbalanced with the variation of input matrix size and density. Compared with HyGCN, we designed a unified architecture with SSMM and SDMM mode, making full use of the computing and memory resources. Thus, we achieve $3.2\times\sim 19.8\times$ performance.

For GCNAX, it applies a row remapping strategy to accumulate psum more regularly, which achieves great performance in SDMM. However, it only exploits the sparsity of one input matrix, which gains less benefits in SSMM. Thus, the performance of GCNAX is $1.1\times\sim 1.4\times$ higher than ours in the SDMM benchmark because the computing flow of SDMM is similar with us but the workload of GCNAX is more balanced with a smaller PE array. If our PE array is scaled to the same size with GCNAX, we can achieve the same performance theoretically. For the SSMM benchmark, we achieve $9.8\times\sim 12.1\times$ speedup in due to sparsity exploiting of two matrices.

For OuterSPACE, although it removes most of the zero element computations in the input matrix through outer product approach, the irregular distribution of non-zero elements in the psum matrix leads to longer accumulation delays. Compared with OuterSPACE, we applied an address mapping method to regularize the psum accumulating. Thus, our performance is $2.9\times\sim 6.4\times$ higher than OuterSPACE.

For SpArch, it condenses the input matrices to reduce the psum matrix and speeds up the accumulation process with the merge tree. However, no data reusing among PEs leads to longer input data loading delays, which can be deteriorative in SDMM. Compared with SpArch, the benefit of optimizing psum accumulation is similar to us, but we reuse the input matrices based on IOHP. Thus, we achieve $1.3\times\sim 4.8\times$ performance compared with SpArch.

6.3 Energy and Resource Efficiency

To demonstrate the benefit of performance outweighs the area and power overhead in IOPS, we compared the energy and resource efficiency with SPOTS, HyGCN, GCNAX, OuterSPACE, and SpArch, achieving $7.2\times\sim 21.9\times$, $6.7\times\sim 41.7\times$, $0.3\times\sim 4.9\times$, $7.9\times\sim 17.1\times$, and $1.7\times\sim 6.3\times$ energy efficiency, respectively, as shown in Fig.12, and achieving $11.9\times\sim 36.3\times$, $1.9\times\sim 11.9\times$, $2.4\times\sim 40\times$, $12.9\times\sim 28\times$, and $1.2\times\sim 4.4\times$ resource efficiency, respectively, as shown in Fig.13. The normalized energy efficiency, E_N , is calculated as $R_{Pr}/(R_w \times s)$, where R_w is the ratio of power of IOPS to other accelerators, and s is the power scalar [32] among different technologies. To explain the difference of architecture design, E_N can be calculated as $(R_{Pr}/R_{Pt})/(R_W/R_{Pt} \times s) = P_N \times E_T$, where the E_T is the top energy efficiency, representing the power consumption per throughput. Similarly, the normalized resource efficiency, R_N , is calculated as $R_N = P_N \times R_T$, where the R_T is the top resource efficiency, representing the area cost per throughput.

For SPOTS, the PE unit of systolic array only consists of one MAC unit and psum buffer, simplifying the structure and leaving out many operations compared with IOPS. However, the imbalanced row and column size of PE array induces more buffers for a higher bandwidth requirement. Besides, the data value of SPOTS are 16-bit fixed point, which needs to scale $4\times$ power and area to match the hardware of 64-bit float point. Thus, our top energy efficiency, E_T , and top resource efficiency, R_T , are $0.5\times$ and $0.83\times$ lower than SPOTS. Combining with the normalized performance, P_N , we achieve $7.2\times\sim 21.9\times$ normalized energy efficiency, E_N , and $11.9\times\sim 36.3\times$ normalized resource efficiency, R_N , respectively.



Fig. 12: Energy efficiency comparison with SPOTS, HyGCN, GCNAX, OuterSPACE, and SpArch.

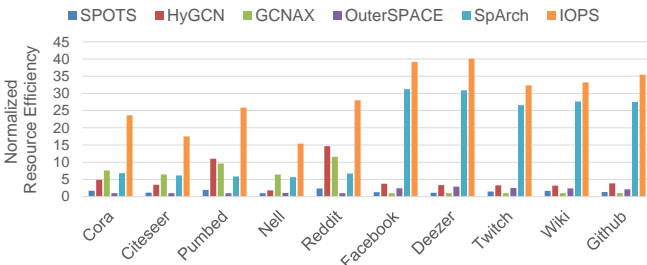


Fig. 13: Resource efficiency comparison with SPOTS, HyGCN, GCNAX, OuterSPACE, and SpArch.

For HyGCN, the DDMM engine based on systolic arrays can achieve higher throughput with lower area, but also consumes more power due to the denser computing units. Besides, the interface between the SDMM and DDMM engine occupies 35% area and 20% power for establishing the pipeline, which is an extra module compared with IOPS. Additionally, the 32-bit fixed point data of HyGCN scales $2\times$ power and area to match with double float point. Therefore, our R_T is $0.7\times$ lower than HyGCN but our E_T is $2.1\times$ higher than it. Finally, our E_N and R_N are $6.7\times\sim 41.7\times$ and $1.9\times\sim 11.9\times$ higher than OuterSPACE, respectively.

For GCNAX, it builds a specialized accelerator for SDMM, which can remove a part of operations in SSMM and consumes less power. However, the 1×16 PE array of GCNAX consumes higher bandwidth on average compared with the 8×8 PE array of IOPS, inducing more storage resources. Thus, we achieve $3.3\times$ R_T compared with GCNAX but our E_T is $0.4\times$ lower than it. Finally, our E_N and R_N are $0.3\times\sim 4.9\times$ and $2.4\times\sim 40\times$ higher than GCNAX, respectively.

For OuterSPACE, its PE structure is more general-purpose, containing many caches and instruction decoding modules, while our architecture is specialized for SpMM with simpler computing flow. Therefore, our E_T and R_T are $2.7\times$ and $4.4\times$ higher than OuterSPACE, respectively. Finally, our energy and resource efficiency are $4.5\times\sim 10.5\times$ and $8.3\times\sim 19.4\times$ higher than OuterSPACE, respectively.

For SpArch, most of power and area are consumed by the merge tree, which is similar with the PE array in IOPS. Both of us aim to relieve the irregularity of psum access. Therefore, our E_T and R_T are $1.3\times$ and $0.9\times$ higher than SpArch, respectively. Combining the performance, our E_N and R_N are $1.7\times\sim 6.3\times$ and $1.2\times\sim 4.4\times$ higher compared with SpArch, respectively.

6.4 DRAM Access

To explore the energy consumption of off-chip data movement, we compare DRAM access saving with SPOTS, HyGCN, GCNAX, OuterSPACE, and SpArch, achieving $7\times\sim 19.1\times$, $2.8\times\sim 12.9\times$, $0.8\times\sim 11.2\times$, $2.2\times\sim 4.4\times$, and $1.2\times\sim 2.7\times$, respectively, as shown in Fig.14. To make a fair comparison, we assume the same on-chip storage to explore the difference of dataflow in each accelerator. The specific parameters of matrix partition are shown in Tab.10, whose meanings have been explained in Tab.5. For SDMM benchmark, we show the partition of two steps in the first layer, where we reuse the sparse matrices A first (RAF) in most case, except for the Pumbed and Reddit dataset with the dense feature matrix. For the SSMM benchmark, we reuse each matrix based on the DRAM access in each case. The average utilization of input buffer is $50\%\sim 75\%$, fully utilizing the buffers without overflowing. Since the psum matrices in SDMM are dense, we can achieve a 100% utilization theoretically.

For SPOTS, though there are many input and output matrices reuse in the PE array, the mismatched index of input matrices induces large amount of zeros and wastes the buffer storage to store the zero element. The more zeros contained in the buffer, the smaller sizes of submatrix are, leading to more tiling blocks and repeat DRAM access of

TABLE 10: Parameters of Matrix Partition

Dataset	Mt	Nt	Kt	Tk	Tm	Tn	Buffer Utilization (A/B/Psum)	Computing Mode	Reuse Strategy
cora	339,339	1,1	2708,287	1,5	1,1	180,2	63%/62%/66%	SDMM,SDMM	RAF,RAF
citeseer	416,416	1,1	3327,412	1,9	1,1	463,2	56%/71%/81%	SDMM,SDMM	RAF,RAF
pumbed	493,4	1,2	9859,500	2,1	5,617	63,1	55%/75%/96%	SDMM, DDMM	RABE,RBF
nell	504,504	1,1	42336,20426	4,3	42,42	7660,8	65%/55%/98%	SDMM, SDMM	RAF,RAF
Reddit	511,10	1,8	1421,201	164,3	57,2912	76,1	74%/74%/91%	SDMM, DDMM	RABE,RAF
Facebook	201	43	11235	2	14	14	75%/71%/74%	SSMM	RAF
Deezer	442	83	14141	2	4	47	67%/63%/67%	SSMM	RAF
Twitch	92	14	9498	1	13	24	72%/53%/75%	SSMM	RBF
Wiki	112	23	5816	2	13	72	41%/74%/70%	SSMM	RBF
Github	197	27	9425	4	24	19	73%/57%/71%	SSMM	RAF

input matrices. Thus, we achieve $7\times\sim 19.1\times$ DRAM access saving.

For HyGCN, the SSMM engine stations the input matrix A and shrinks the submatrix size to reduce the sparsity. Then, it repeatedly loads the corresponding element of input matrix B. However, for the SDMM benchmark, the execution order brings more computation with more data access from DRAM. For the SSMM benchmark, the output matrix is stored in a dense format as the input for DDMM engine, causing the storage waste and lowering the data reusing rate. Therefore, we reduce $2.8\times\sim 12.9\times$ DRAM access.

For GCNAX, it reuses the sparse matrix and repeatedly accesses the dense matrix in the SDMM computing, similar to our approach in this case. However, for the SSMM benchmark, the accumulated psum matrix can contain many zero elements, which limits the sizes of output submatrices. The DRAM access can be more frequent due to more tiling blocks. Thus, we achieve $0.8\times\sim 11.2\times$ DRAM access saving.

For OuterSPACE, the main DRAM access comes from the irregular psum accumulation. Compared with OuterSPACE, we relieve the irregularity of the psum access by applying address mapping, which obtains the final output matrix on-chip without repeat DRAM access. Therefore, we achieve $2.2\times\sim 4.4\times$ DRAM access saving.

For SpArch, it reduces the psum matrix by a Huffman tree scheduler and merges the psum to calculate final output matrix, greatly reducing the DRAM access of psum accumulation. However, there is no input reuse between each PE, which causes more repeat access of input matrix and gets worse in the SDMM benchmark. Besides, we reorganize the psum buffer for $2\times$ storage in SDMM, reducing DRAM access further. Thus, we reduce $1.2\times\sim 2.7\times$ DRAM access.

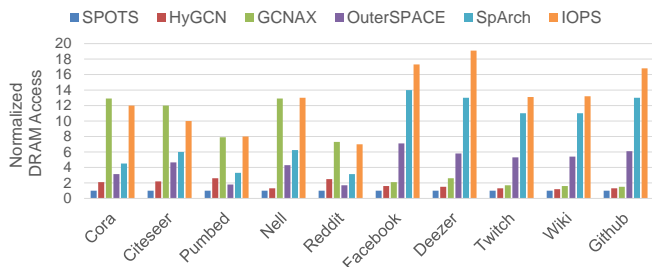


Fig. 14: DRAM access comparison with SPOTS, OuterSPACE, HyGCN, GCNAX, and SpArch.

7 DESIGN SPACE EXPLORATION

To explore the influence of hardware parameters on performance, energy efficiency, and resource efficiency, we testify the IOPS with different PE array size and buffer storage, as shown in Fig.15 and Fig.16. Since the DRAM access is mainly determined by the dataflow, there is no need to explore in the same architecture. For the PE array size, $G_{NAX}G_{NB}$, the area of PE array and input buffer in the architecture are scaled by square and linearity, respectively, indicating that the larger $G_{NAX}G_{NB}$ is, the higher E_T and R_T we achieve. However, with the increasing of PE array size, the density of each submatrix in each PE can be more imbalanced, causing performance degradation. Thus, we set three different $G_{NAX}G_{NB}$, 4×4 , 8×8 , and 16×16 , to explore their difference. As shown in Fig.15, the 8×8 PE array achieves $0.56\times\sim 0.92\times$ performance with $1.35\times E_T$ and $1.5\times R_T$ compared with 4×4 PE array, and achieves $1.15\times\sim 1.68\times$ performance with $0.91\times E_T$ and $0.83\times R_T$ compared with 16×16 PE array. Considering the final E_N and R_N , 8×8 PE array performs better in these benchmarks.

For the buffer storage, the larger submatrix we can store, the more balanced density of each submatrix is, indicating higher performance. However, with larger buffer comes more resource and power overhead. Thus, we shrink and magnify the input buffer $2\times$ (psum buffer $4\times$) to testify the benchmark, where the E_T of $2\times$ buffer and $0.5\times$ buffer are $0.63\times$ and $1.2\times$ that of the basic buffer, respectively, and the R_T are $0.4\times$ and $1.7\times$, respectively. Combining with the P_N , the E_N of $1\times$ buffer is $1.3\times\sim 2.1\times$ and $0.76\times\sim 1.3\times$ higher than $0.5\times$ buffer and $2\times$ buffer, respectively, and the R_N is $0.86\times\sim 1.5\times$ and $1.2\times\sim 2.1\times$, respectively. Therefore, we choose $1\times$ buffer for the balance of performance and hardware overhead.

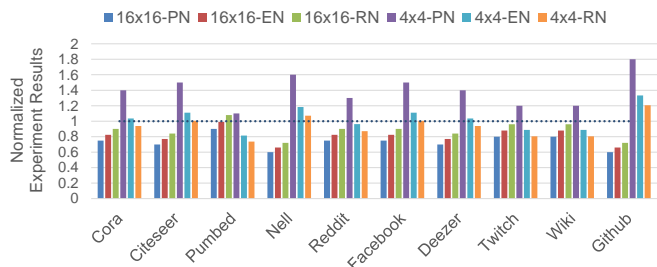


Fig. 15: Experiment results comparison among different PE array sizes.

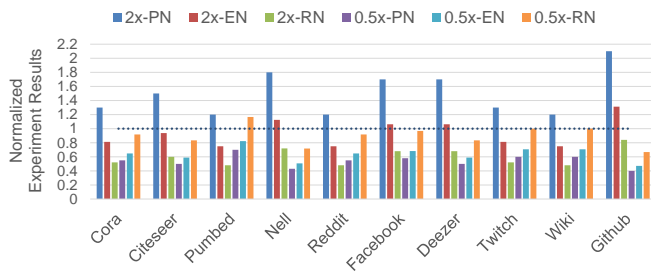


Fig. 16: Experiment results comparison among different buffer storages.

8 CONCLUSION

This paper proposes an IOHP based accelerator for SpMM, which reuses the input matrix across PEs with inner product based dataflow, and removes zero-element calculations based on outer product. Besides, an address mapping method is designed to address the irregularity of DRAM access during psum accumulation. Furthermore, an adaptive partition strategy is proposed to tile the input matrices based on their sparsity ratio, effectively utilizing the storage of architecture and reducing DRAM access. Collaborating with the above method, this accelerator can switch the computing mode between the SSMM and SDMM efficiently. Compared with SpArch, we achieve $1.7\times\sim 6.3\times$ energy efficiency and $1.2\times\sim 4.4\times$ resource efficiency, with $1.4\times\sim 2.1\times$ DRAM access saving.

REFERENCES

- [1] P. D'alberto and A. Nicolau, "R-klene: A high-performance divide-and-conquer algorithm for the all-pair shortest path for densely connected networks," *Algorithmica*, vol. 47, no. 2, p. 203–213, feb 2007.
- [2] R. Ying, R. He, and et al, "Graph convolutional neural networks for web-scale recommender systems," in *ACM KDD*, 2018, p. 974–983.
- [3] S. Goedecker and L. Colombo, "Tight binding molecular dynamics on parallel computers," USA, Tech. Rep., 1994.
- [4] T. N. Kipf and M. Welling, "Semi-supervised classification with graph convolutional networks," in *arXiv*, 2017. [Online]. Available: <https://arxiv.org/abs/1609.02907>
- [5] J. Leskovec and A. Krevl, "SNAP Datasets: Stanford large network dataset collection," <http://snap.stanford.edu/data>, Jun. 2014.
- [6] N. P. Jouppi, C. Young, and et al, "In-datacenter performance analysis of a tensor processing unit," in *ISCA*, 2017, pp. 1–12.
- [7] G. Jeong, E. Qin, and et al, "Rasa: Efficient register-aware systolic array matrix engine for cpu," in *DAC*, 2021, pp. 253–258.
- [8] Y. Zhu and et al, "Exploiting parallelism with vertex-clustering in processing-in-memory-based gcn accelerators," in *DATE*, 2022, pp. 652–657.
- [9] —, "Exploiting parallelism with vertex-clustering in processing-in-memory-based gcn accelerators," in *DATE*, 2022, pp. 652–657.
- [10] M. Yan, L. Deng, X. Hu, L. Liang, Y. Feng, X. Ye, Z. Zhang, D. Fan, and Y. Xie, "Hygcn: A gcn accelerator with hybrid architecture," in *2020 IEEE International Symposium on High Performance Computer Architecture (HPCA)*, 2020, pp. 15–29.
- [11] M. Soltanyeh and et al, "An accelerator for sparse convolutional neural networks leveraging systolic general matrix-matrix multiplication," *ACM Trans. Archit. Code Optim.*, vol. 19, no. 3, may 2022.
- [12] S. Dalton, L. Olson, and N. Bell, "Optimizing sparse matrix-matrix multiplication for the gpu," *ACM Trans. Math. Softw.*, vol. 41, no. 4, oct 2015. [Online]. Available: <https://doi.org/10.1145/2699470>

- [13] W. Liu and B. Vinter, "An efficient gpu general sparse matrix-matrix multiplication for irregular data," in *2014 IEEE 28th International Parallel and Distributed Processing Symposium*, 2014, pp. 370–381.
- [14] J. Lee, Kang, and et al, "Optimization of gpu-based sparse matrix multiplication for large sparse networks," in *ICDE*, 2020, pp. 925–936.
- [15] N. G. N. S. and K. S., "Moscon: Modified outer product based sparse matrix-matrix multiplication accelerator with configurable tiles," in *VLSID*, 2023, pp. 264–269.
- [16] S. Pal, J. Beaumont, and et al, "Outerspace: An outer product based sparse matrix multiplication accelerator," in *HPCA*, 2018, pp. 724–736.
- [17] Z. Zhang, H. Wang, and et al, "Sparch: Efficient architecture for sparse matrix multiplication," in *HPCA*, 2020, pp. 261–274.
- [18] T. Geng, A. Li, R. Shi, C. Wu, T. Wang, Y. Li, P. Haghi, A. Tumeo, S. Che, S. Reinhardt, and M. C. Herbordt, "Awb-gcn: A graph convolutional network accelerator with runtime workload rebalancing," in *2020 53rd Annual IEEE/ACM International Symposium on Microarchitecture (MICRO)*, 2020, pp. 922–936.
- [19] J. Li, A. Louri, A. Karanth, and R. Bunesco, "Gcnax: A flexible and energy-efficient accelerator for graph convolutional neural networks," in *2021 IEEE International Symposium on High-Performance Computer Architecture (HPCA)*, 2021, pp. 775–788.
- [20] N. Srivastava, H. Jin, and et al, "Matraprot: A sparse-sparse matrix multiplication accelerator based on row-wise product," in *MICRO*, 2020, pp. 766–780.
- [21] H. Kaplan, M. Sharir, and E. Verbin, "Colored intersection searching via sparse rectangular matrix multiplication," in *Proceedings of the Twenty-Second Annual Symposium on Computational Geometry*, ser. SCG '06. New York, NY, USA: Association for Computing Machinery, 2006, p. 52–60. [Online]. Available: <https://doi.org/10.1145/1137856.1137866>
- [22] J. R. Gilbert, S. Reinhardt, and V. B. Shah, "A unified framework for numerical and combinatorial computing," *Computing in Science and Engg.*, vol. 10, no. 2, p. 20–25, mar 2008. [Online]. Available: <https://doi.org/10.1109/MCSE.2008.45>
- [23] M. O. Rabin and V. V. Vazirani, "Maximum matchings in general graphs through randomization," *Journal of Algorithms*, vol. 10, no. 4, pp. 557–567, 1989. [Online]. Available: <https://www.sciencedirect.com/science/article/pii/0196677489900059>
- [24] W. L. Hamilton, R. Ying, and J. Leskovec, "Inductive representation learning on large graphs," in *Proceedings of the 31st International Conference on Neural Information Processing Systems*, ser. NIPS'17. Red Hook, NY, USA: Curran Associates Inc., 2017, p. 1025–1035.
- [25] K. Xu, W. Hu, J. Leskovec, and S. Jegelka, "How powerful are graph neural networks?" *ArXiv*, vol. abs/1810.00826, 2018. [Online]. Available: <https://arxiv.org/abs/1810.00826>
- [26] P. Veličković, G. Cucurull, A. Casanova, A. Romero, P. Liò, and Y. Bengio, "Graph attention networks," 2018. [Online]. Available: <https://arxiv.org/abs/1710.10903>
- [27] A. McCallum, "Cora," <http://www.cs.umd.edu/~sen/lbc-proj/LBC.html>.
- [28] C. L. Giles, K. D. Bollacker, and S. Lawrence, "Citeseer: An automatic citation indexing system," in *Proceedings of the Third ACM Conference on Digital Libraries*, ser. DL '98, 1998, p. 89–98.
- [29] P. Sen, G. Namata, and et al, "Collective classification in network data," in *The AI Magazine*, 2008.
- [30] A. Carlson, J. Betteridge, and et al, "Toward an architecture for never-ending language learning," in *Proceedings of the Twenty-Fourth AAAI Conference on Artificial Intelligence*. AAAI Press, 2010, p. 1306–1313.
- [31] P. Yanardag and S. Vishwanathan, "Deep graph kernels," in *Proceedings of the 21th ACM SIGKDD International Conference on Knowledge Discovery and Data Mining*, ser. KDD '15. New York, NY, USA: Association for Computing Machinery, 2015, p. 1365–1374. [Online]. Available: <https://doi.org/10.1145/2783258.2783417>
- [32] O. Villa, D. R. Johnson, M. Oconnor, E. Bolotin, D. Nellans, J. Luitjens, N. Sakharnykh, P. Wang, P. Micikevicius, A. Scudiero, S. W. Keckler, and W. J. Dally, "Scaling the power wall: A path to exascale," in *SC '14: Proceedings of the International Conference for High Performance Computing, Networking, Storage and Analysis*, 2014, pp. 830–841.